RSC Advances

PAPER

View Article Online
View Journal | View Issue

Cite this: *RSC Adv.*, 2024, **14**, 6603

Adsorption of hexavalent chromium from wastewater using polyaniline-coated microcrystalline cellulose nanocomposites

Lovejoy Dewa,[a] Shepherd Masimba Tichapondwa[b] and Washington Mhike *[a]

In this study, the effectiveness of microcrystalline cellulose (MCC) as an adsorbent for the removal of hexavalent chromium, Cr(VI), from synthetic wastewater was enhanced through functionalization with polyaniline (PANI). Scanning electron microscopy (SEM) showed that MCC was an effective scaffold for *in situ* chemical oxidative polymerization of aniline. Fourier transform infrared spectroscopy (FTIR) spectroscopy and X-ray diffraction confirmed successful PANI synthesis. The MCC/PANI nanocomposites exhibited relatively high specific surface areas, compared to that of the MCC (2.05 m^2 g^{-1}). Batch adsorption studies showed that the optimal conditions for the removal of Cr(VI) from wastewater using the MCC/PANI-69 wt% nanocomposite were an initial Cr(VI) concentration of 100 mg L^{-1}, an adsorbent dosage of 4 g L^{-1} and a Cr(VI) solution pH of 7. The MCC/PANI-69 wt% required only 30 min to reach equilibrium and the equilibrium removal efficiency was 95%. FTIR spectroscopy and energy dispersive X-ray spectrometry results suggest that the Cr(VI) removal mechanism by the MCC/PANI-69 wt% nanocomposite at pH 7 was through electrostatic attraction of Cr(VI) species by PANI, reduction of Cr(VI) into Cr(III) and precipitation of Cr(III) on the nanocomposite surface. The kinetics for the removal of the Cr(VI) by the MCC/PANI-69 wt% nanocomposite were adequately described by the pseudo second order (PSO) kinetics model, whereas the Langmuir isotherm adequately described the equilibrium data. The MCC/PANI-69 wt% nanocomposite had a significantly improved maximum adsorption capacity of 35.97 mg g^{-1}, at pH 7, in comparison to that of the MCC (3.92 mg g^{-1} at pH 1). The study demonstrated that, whereas most of the reported adsorbents for Cr(VI) are only effective at low pH values, the MCC/PANI nanocomposite synthesized in this study was effective at pH 7.

Received 23rd November 2023
Accepted 16th February 2024

DOI: 10.1039/d3ra08027g

rsc.li/rsc-advances

1 Introduction

Cr(VI) is a highly toxic and persistent pollutant in aqueous environments due to its oxidizing strength, solubility, non-biodegradability and mobility.[1] Various industrial and anthropogenic activities contribute to Cr(VI) pollution of freshwater bodies. For instance, processes which are used in the ferrochrome industry unintentionally generate Cr(VI)- containing waste and wastewater that contaminate fresh water bodies.[2] Cr(VI) compounds are also widely used in leather tanning, manufacture of pigments, electroplating, manufacture of chromic acid and speciality chemicals.[3] Lack of treatment or inadequate treatment of Cr(VI) effluents which are then discharged into fresh water bodies are the main causes of Cr(VI) pollution of freshwater sources.[4–6]

Presently, most of the available water treatment methods are not capable of effectively removing Cr(VI) present in water at trace concentration levels.[7] These processes also have several other disadvantages.[2,8,9]

In an effort to meet stringent regulations such as the maximum limit of 0.05 mg L^{-1} for Cr(VI) in drinking water recommended by the World Health Organization (WHO), adsorption has drawn immense interest.[7,10] Adsorption is considered as an effective, efficient and economic remediation method for heavy metal contaminated water and wastewater which offers flexibility in design and operation. In some instances, it might also be possible to regenerate the adsorbents.[11] However, the feasibility and cost effectiveness of adsorption in water treatment is dependent on the availability of low cost, high selective and efficient adsorbents.[12] Conventional commercial adsorbents such as activated carbons, silica gel, activated alumina, zeolites, clays are relatively expensive for remediation of Cr(VI) present in water in trace quantities.[7,12]

Alternative non-conventional adsorbents which are products and by-products of biological, industrial processes and of agricultural origin have been proposed and studied as

[a]*Polymer Technology Division, Department of Chemical, Metallurgical and Materials Engineering, Tshwane University of Technology, Pretoria 0001, South Africa. E-mail: MhikeW@tut.ac.za; Tel: +27 12 382 5460*

[b]*Water Utilization Division, Department of Chemical Engineering, University of Pretoria, Pretoria 0001, South Africa*

inexpensive and efficient adsorbents.[13] Several microbial, plant and animal biomasses and their derivatives have been studied as biosorbents, adsorbents that are based on biological matrices (biomass). These include polysaccharides such as starch, chitin, chitosan and cellulose.[14]

Compared to conventional adsorbents, biosorbents are relatively inexpensive, readily available in large quantities and abundant in nature. They are potentially able to remove heavy metals from water with minimal generation of toxic sludge. However, their greatest advantage is that they are environmentally friendly as they are biodegradable, and thus they are easily disposed, after use.[13–15] Several studies have demonstrated the effectiveness of plant-based biosorbents in the removal of Cr(VI).[13]

Cellulose is the most abundant natural polymer on earth.[16] It is a semicrystalline polysaccharide that contains hydroxyl functional groups on its molecular chain structure. Microcrystalline cellulose (MCC) is purified, partially depolymerized cellulose.[17] Cellulose-based materials are often considered for use as biosorbents due to their relatively low cost and abundance.[18]

Cellulose and similarly MCC, lack functional groups that are able to complex heavy metals and other pollutants. As a result, there have been a few studies on the use of pristine MCC as an adsorbent.[19] However, the prevalence of hydroxyl groups on cellulose and MCC structures enables them to be modified and functionalized to target specific pollutants.[20]

Polyaniline (PANI) is one of the most widely studied intrinsically conducting polymers (ICP).[21] PANI has also been studied as an adsorbent for water treatment.[22] Its monomer is relatively inexpensive, it is easily synthesized and tuned.[21] PANI contains amine and imine functional groups that are able to interact with some metal ions and other pollutants due to their strong affinity to nitrogen atoms. Hence PANI is highly efficient in removing heavy metals from aqueous solutions.[23] However, its particles easily aggregate during their synthesis. This reduces its specific area and limits its adsorption capacity and practical application. The regeneration of PANI particles is also a challenge.[23] PANI particles are also difficult to disperse in aqueous media.[24] The fabrication of nanocomposites of PANI with other adsorbents has been explored as a solution towards adsorbents with better adsorption capacities, chemical and thermal stability, good regeneration ability, and selectivity towards heavy metals.[23]

The aim of this study was to develop inexpensive, effective adsorbents for wastewater treatment based on cellulose. The objective of the study was to enhance the effectiveness of MCC in the removal of Cr(VI), from wastewater through its modification and functionalization with PANI. In the study, MCC was coated with PANI through *in situ* chemical oxidative polymerization of aniline. The PANI coated MCC was then applied in batch adsorption studies on the removal of Cr(VI) from synthetic wastewater.

This work introduces a novel work of fabricating MCC/PANI nanocomposites through *in situ* polymerization of PANI, thereby utilizing MCC as an effect scaffold for the synthesis of PANI. It is envisaged that the study will contribute to the development of biodegradable, cost effective and efficient biosorbents for the removal of Cr(VI) at neutral pH.

2 Materials and methods

2.1 Materials

The MCC used in the study was grade Avicel 101 with a d_{50} particle size of 65 μm supplied by JRS Pharma industry, India. Aniline (99.5%), *para*-toluene sulphonic acid (98.5%) and 1,5-diphenylcarbazide (98.0%) were supplied by Sigma Aldrich, South Africa. Ammonium persulphate (99.0%), potassium chromate (99.0%), hydrochloric acid (37%), ethanol (99.9%), acetone (AR) and sodium hydroxide pellets (98%) were supplied by Glassworld, South Africa. All the reagents were of analytical grade and were used as received. All solutions were prepared with deionized water.

2.2 Methods

2.2.1 Synthesis of PANI and MCC/PANI nanocomposites. PANI was synthesized through chemical oxidative polymerization of aniline in aqueous acidic media using ammonium persulphate (APS) as the oxidant, according to the reaction scheme proposed by Stejskal *et al.*[25] 3.8 g of *para*-toluene sulfonic acid (PTSA) was dissolved in 400 mL of deionized water. Aniline (2 mL) was then added to the acidic solution. APS (2.5 g) was separately dissolved in 50 mL of deionized water. Both mixtures were cooled to 0 °C in an ice bath, and then the APS solution was added dropwise to the aniline/PTSA solution. The reaction mixture was left overnight under constant stirring. The completion of the reaction was indicated by the colour change of the reaction mixture, from colourless to dark green, signifying the presence of the emeraldine salt. Subsequently, the reaction mixture was vacuum filtrated through a mixed cellulose ester filter (0.45 μm pore size, Whatman Co., Germany). The filtrate was then washed several times with deionized water, and then with ethanol. Finally, the PANI was scrapped off from the filter paper, dried in a vacuum oven at 60 °C for 24 h and then stored in an air-tight container for further experiments.

The MCC/PANI nanocomposites were prepared *via in situ* chemical oxidative polymerization of aniline in the presence of MCC. The compositions of the MCC/PANI nanocomposites which were synthesized in the study ranged from 9–75 wt% PANI, these are shown in Table 1. 5 g of MCC was used in the preparation of each nanocomposite. The PANI formed in this study was assumed to be completely protonated. It was also assumed that the protonated nitrogen atoms were associated with counter anions from the PTSA dopant.[25] Hence the repeat unit molecular weight of the PANI-PTSA was determined as 706 g mol^{-1}, which enabled the determination of the theoretical mass of PANI formed, using the reaction scheme proposed by Stejskal *et al.*[25] In the synthesis of each nanocomposite, an appropriate amount of ammonium persulfate (APS) powder corresponding to a molar ratio of 1.25 with respect to aniline was separately completely dissolved in 50 mL of deionized water by stirring. The polymerization was then conducted as described in the paragraph above.

2.2.2 Characterization of the MCC and MCC/PANI nanocomposites. The functional groups on the MCC, PANI and the MCC/PANI nanocomposites were studied through FTIR

Table 1 MCC/PANI nanocomposites formulations

Sample	PANI (wt%)	Aniline (mL)	Aniline (mol)	APS (mol)	APS (g)	PANI (mol)	PANI (g)
MCC/PANI-9 wt%	9	0.25	0.00269	0.00336	0.766	0.00067	0.47
MCC/PANI-16 wt%	16	0.50	0.00538	0.00672	1.532	0.00134	0.95
MCC/PANI-28 wt%	28	1.00	0.01075	0.01344	3.065	0.00269	1.90
MCC/PANI-36 wt%	36	1.50	0.01613	0.02016	4.597	0.00403	2.85
MCC/PANI-43 wt%	43	2.00	0.02151	0.02688	6.129	0.00538	3.80
MCC/PANI-53 wt%	53	3.00	0.03226	0.04032	9.194	0.00806	5.69
MCC/PANI-60 wt%	60	4.00	0.04301	0.05376	12.258	0.01075	7.59
MCC/PANI-65 wt%	65	5.00	0.05376	0.06720	15.323	0.01344	9.49
MCC/PANI-69 wt%	69	6.00	0.06452	0.08065	18.387	0.01613	11.39
MCC/PANI-75 wt%	75	8.00	0.08602	0.10753	24.516	0.02151	15.18

spectroscopy. The FTIR spectra were recorded on a PerkinElmer 100 FTIR spectrophotometer equipped with an attenuated total reflectance accessory in the range 4000–600 cm^{-1}, using 64 scans and a resolution of 4 cm^{-1}.

The morphologies of the neat MCC, PANI and the MCC/PANI nanocomposites were analysed on a ZEISS crossbeam 540 field emission gun scanning electron microscope (FESEM) using an accelerating voltage of 2.0 kV. Elemental compositions of the materials were analysed using energy dispersive X-ray (EDX) spectrometry coupled to the FESEM. The specific surface area and pore characteristics of the MCC, PANI and the MCC/PANI nanocomposites were evaluated using a Micromeritics TriStar II surface area and porosity analyser. The crystallinity of the MCC, PANI and the MCC/PANI nanocomposites was analysed using a PAnalytical X'Pert Pro powder X-ray diffractometer using Cu-Kα radiation in the 2θ range 0° and 90°. The point of zero charge (pHpzc) of the MCC was determined by the salt addition method as described by Bakatula *et al.*[26]

2.2.3 Adsorption of Cr(VI) by MCC. Stock solutions of 1000 mg L^{-1} Cr(VI) were prepared by dissolving 3.7344 g of K_2CrO_4 in 1 L of deionized water. Varying concentrations of the synthetic wastewater containing Cr(VI) (chromate solution) were then obtained by dilution of the stock solutions with deionized water.

Batch adsorption experiments were conducted at standard room temperature conditions using the MCC as an adsobent for the removal of Cr(VI) from the synthetic wastewater. All experiments were conducted in duplicates and the average results reported. The experiments were conducted in 250 mL glass bottles using 50 mL of the Cr(VI) solution. The bottles were agitated at 150 rpm using a mechanical shaker for a predetermined period obtained from initial kinetics results. Process parameters such as the adsobent dosage, initial Cr(VI) concentrations, contact time, and solution pH were optimized by changing one variable at a time and maintaining all the others constant.

The Cr(VI) residual concentrations in the synthetic wastewater after adsorption were determined using the standard ultraviolet-visible (UV-Vis) spectrophotometric method described by Eaton and Franson using a WPA, Lightwave II, Labotec UV-Vis spectrophotometer at a wavelength of 540 nm.[27]

The maximum amount of Cr(VI) adsorbed by the MCC adsorbent for each run, were determined using eqn (1):

$$q_e = \frac{(C_0 - C_e)V}{W} \quad (1)$$

where q_e (mg g^{-1}) is the equilibrium the adsorption capacity, C_0 (mg L^{-1}) is the initial concentration of Cr(VI), C_e (mg L^{-1}) is the equilibrium concentration of Cr(VI), V (L) is the volume of the Cr(VI) solution and W (g) is the mass of MCC or MCC/PANI nanocomposite added. The Cr(VI) removal efficiency R (%) was determined using eqn (2):

$$R = \left(\frac{C_0 - C_e}{C_0}\right) \times 100 \quad (2)$$

where the concentrations are as defined above.

To study the effect of the MCC dosage on the removal of Cr(VI), the amount of MCC was varied from 2.5 g L^{-1} to 80 g L^{-1}. In this experiment, the initial concentration of the chromate solution was kept constant at 10 mg L^{-1}, a contact time of 120 h was used, based on the initial kinetics results. The optimum MCC dosage which yielded the best removal efficiency/capacity was 20 g L^{-1}, this was used in subsequent experiments.

The MCC maximum adsorption capacity for Cr(VI) was determined through equilibrium isotherm studies. These were carried out using varying initial concentrations of Cr(VI) solutions which ranged from 10 to 100 mg L^{-1} while maintaining the MCC dosage at the determined optimum loading of 20 g L^{-1}. The effect of solution pH on the removal of Cr(VI) from solution by the MCC was investigated in the pH range 1–9, using a Cr(VI) concentration of 10 mg L^{-1} and the determined MCC optimum loading of 20 g L^{-1}. The pH of the solution was adjusted by addition of HCl or NaOH solution (0.01–5.0 mol L^{-1}) using a pH meter with a resolution of ±0.05 pH.

Batch adsorption kinetics data for the adsorption of Cr(VI) by MCC were obtained by varying the contact time from 0–144 h with an initial Cr(VI) concentration of 10 mg L^{-1} and adsorbent dosage of 20 g L^{-1}.

2.2.4 Adsorption of Cr(VI) by MCC/PANI nanocomposites. The effect of the PANI content of the MCC/PANI nanocomposite on the Cr(VI) removal from the synthetic wastewater was investigated by using 100 mg of each of the synthesized MCC/PANI nanocomposites to treat 50 mL of 100 mg L^{-1} of the Cr(VI) solution at pH 7 for 24 h. After the 24 h period, solutions were drawn from the supernatant for the determination of residual Cr(VI) concentrations using the UV-Vis spectrophotometric

method described in §2.2.2. Based on the Cr(VI) removal efficiency of each of the prepared nanocomposites, the 69 wt% PANI nanocomposite (MCC/PANI-69 wt%) was selected for further studies on the Cr(VI) removal from solution. For comparison, the as-received MCC (100 mg) was used to treat 50 mL Cr(VI) solution at pH 7.0 with an initial Cr(VI) concentration of 100 mg L^{-1} for 24 h.

The effect of the MCC/PANI nanocomposites adsorbent dosage on the Cr(VI) removal was studied by using varying amounts of the 69 wt% PANI nanocomposite (MCC/PANI-69 wt%) to treat 50 mL synthetic wastewater with a concentration of 100 mg L^{-1} Cr(VI) concentration at pH 7 for 24 h. An optimum adsobent dosage of 4 g L^{-1} was selected for further studies, after these experiments.

The effect of the contact time on the removal of Cr(VI) by the MCC/PANI-69 wt% nanocomposite was studied in the range 0–180 min at pH 7 and room temperature in order to determine the adsorption kinetics. 200 mg of the MCC/PANI-69 wt% nanocomposite was mixed with 50 mL of Cr(VI) solution in 250 mL glass bottles having concentrations of 100, 200 and 300 mg L^{-1}. The bottles were then agitated at 150 rpm using a mechanical shaker. Samples were drawn at various time intervals and the residual Cr(VI) concentration was analysed using the UV-Vis spectrophotometric method described in §2.2.2. The removal efficiency at different time intervals was determined using eqn (2).

The effect of the initial Cr(VI) concentration on the removal of Cr(VI) from the synthetic wastewater by the MCC/PANI-69 wt% nanocomposite was studied in the Cr(VI) solution concentration range 100–500 mg L^{-1}, leading to the determination of the adsorption isotherms. This was done by using the optimum MCC/PANI-69 wt% nanocomposite adsorbent dosage of 4 g L^{-1} to treat the Cr(VI) solution at pH 7. To attain equilibrium, the glass bottles containing the adsorbent and the Cr(VI) solution were agitated on a shaker at 150 rpm for 180 min. After equilibrium was attained, the residual Cr(VI) concentration was analysed using the UV-Vis spectrophotometric method described in §2.2.2. To determine the amount of Cr(VI) adsorbed, the equilibrium adsorption capacity was calculated using eqn (1). All experiments were conducted in duplicates and the average results reported.

3 Results and discussion

3.1 Characterization of the MCC, PANI and MCC/PANI nanocomposites

3.1.1 Fourier transform infrared spectroscopy (FTIR). FTIR spectroscopy was used to study the functional groups on the pristine MCC and PANI surfaces, and their nanocomposites. Fig. 1 shows the FTIR spectra of the MCC, PANI, and the MCC/PANI nanocomposites with PANI content varying from 9 to 75 wt%. The main characteristic infrared absorption bands of cellulose where identified in the FTIR spectrum of the MCC used in this study as elaborated in Mhike *et al.*[19]

Fig. 1 also shows the FTIR spectra of the *p*-toluene sulphonic acid (PTSA) doped polyaniline (PANI) synthesized in this study. The FTIR spectra of the PANI/PTSA salt in Fig. 1 shows several characteristic infrared adsorption bands exhibited by PANI salts, confirming successful synthesis of PANI in this study.[28] The FTIR spectra bands corresponding to N–H vibrations in PANI were observed in the range 3400–3200 cm^{-1}.[29] In the FTIR spectra of the PANI/PTSA salt in Fig. 1, the band at *ca.* 3230 cm^{-1} is attributed to the protonated amine segments in PANI. The bands at *ca.* 1560 and 1460 cm^{-1} are ascribed to the ring stretching of the quinoid (N=Q=N) and benzenoid (N–B–N) structures in PANI, respectively. B and Q denote benzenoid and quinoid moieties in the PANI chains.[28] The bands at *ca.* 1284 and 1240 cm^{-1} are due to the C–N stretching of aromatic amines in PANI.[28] The band at about *ca.* 1000 cm^{-1} was attributed to vibrational modes of $B–H^{+}=Q$ or $B–NH^{+}–B$, formed during PANI doping reactions.[24] This band is due to the interaction between the PANI polymer chain and the dopant (PTSA).[30] The band at *ca.* 790 cm^{-1} corresponds to the out of plane bending vibration of the C–H aromatic bond in the 1,4 disubstituted benzene ring.[24] The band at *ca.* 670 cm^{-1} was due to the vibrations of the S–O groups in the dopant, PTSA.[30]

Fig. 1 shows that the intensity of the infrared absorption band at *ca.* 3350 cm^{-1} attributed to the stretching of OH groups in MCC decreased with an increase in the PANI content of the MCC/PANI nanocomposites. This observation implies that there was interfacial interaction between the OH groups of the MCC and the PANI, possibly through hydrogen bonding with the PANI nitrogen groups. Li *et al.* previously showed using X-ray photoelectron spectroscopy that PANI and cellulose interacted through hydrogen bonding, demonstrating their good compatibility which is expected to stabilize the nanocomposites in aqueous media.[31] Fig. 1 also shows that the intensity of the band at *ca.* 3230 cm^{-1} attributed to the protonated amine segments in PANI increased with an increase in the PANI content of the nanocomposites.

Another observation from Fig. 1 was that the band at *ca* 1000 cm^{-1} observed in PANI narrowed as the MCC content of the nanocomposites was increased. As discussed in the preceding paragraph, this band was an indication of the occurrence of protonated amine/imine groups in the PANI.

3.1.2 Brunauer–Emmett–Teller (BET) analysis. BET analysis was utilized to determine the specific surface areas and porosities of the MCC, PANI and the MCC/PANI nanocomposites which are presented in Table 2. Table 2 shows that the BET specific surface area of PANI was more than 13 times higher than that of the MCC. Polyaniline can assume various morphologies depending on its synthesis conditions, including nanostructures.[32]

If nanostructures were formed in the synthesis, these would have higher specific areas. Table 2 also shows that PANI had a total pore volume 15 times more than that of the MCC. The BET specific surface areas and total pore volumes of the MCC/PANI nanocomposites were significantly higher than that of the MCC. Table 2 shows that the BET specific surface areas and total pore volumes of the MCC/PANI nanocomposites increased with an increase in the PANI content.

3.1.3 Scanning electron microscopy (SEM). The morphology of the MCC, PANI and MCC/PANI nanocomposites was studied through SEM. Fig. 2 shows the SEM micrographs of

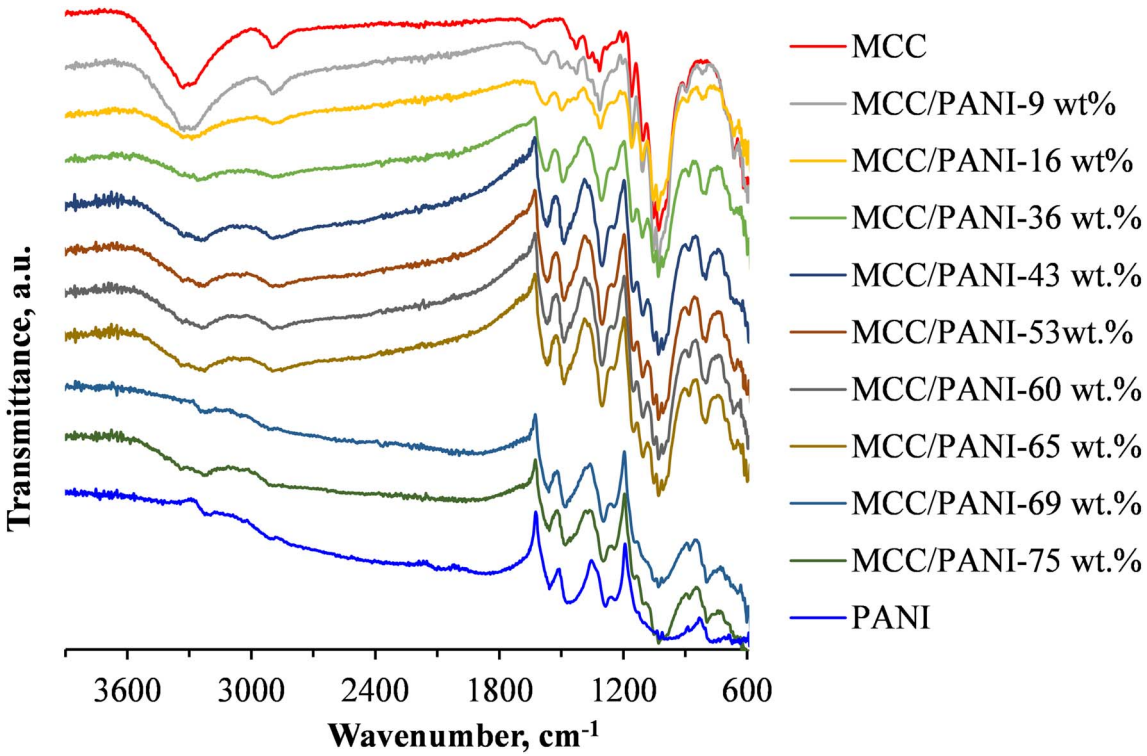

Fig. 1 FTIR spectra of MCC, PANI and MCC/PANI nanocomposites.

Table 2 BET surface areas of MCC, PANI and selected MCC/PANI nanocomposites

Sample	BET surface area, $m^2\ g^{-1}$	Total pore volume, $cm^3\ g^{-1}$
MCC	2.05	0.007925
MCC/PANI-28 wt%	12.08	0.062885
MCC/PANI-53 wt%	22.90	0.110594
MCC/PANI-69 wt%	29.78	0.115668
PANI	27.80	0.123548

MCC, PANI and the MCC/PANI nanocomposites. The morphology of the MCC used in this study shows relatively smooth surfaces.

Fig. 2 also shows that the PANI synthesized in this study consisted of agglomerated nanospheres whose size was estimated at less than 100 nm diameter. The morphology of the PANI observed in Fig. 2 (nanosized spheres) correlates with the relatively high specific surface areas observed for the PANI in the preceding section.

Fig. 2 also shows that as the PANI content in the MCC/PANI nanocomposites was increased up to 28 wt% PANI, the PANI uniformly coated the MCC, suggesting that MCC acted as a scaffold for the PANI synthesis. This appears to be further evidence of good interfacial interaction between the PANI and the MCC, as was suggested in the discussion on the FTIR results in §3.1.1. Beyond 28 wt% PANI content, the MCC surfaces were completely covered by agglomerates of PANI nanospheres. The agglomerated PANI particles on the MCC surface provide an explanation for the increase in specific area of the MCC/PANI nanocomposites observed with an increase in the PANI content.

3.1.4 X-ray diffraction (XRD) analysis. The XRD patterns of the MCC, PANI and MCC/PANI nanocomposites are shown in Fig. 3. The XRD pattern of the MCC in Fig. 4 shows poorly resolved characteristic cellulose diffraction peaks at 2θ *ca.* 16°, 26° and 40° which correspond to reflections by the (110), (200) and (004) planes of cellulose I.[33] This confirms that the MCC was semi-crystalline, it also contained some amorphous regions. The XRD pattern of PANI shown in Fig. 3 exhibits the two main characteristic diffraction peaks observed for PANI, at 2θ *ca.* 23° and 30°. These peaks confirm that the PANI synthesised in this study was in the form of the emaraldine salt.[24] The broad peaks exhibited by PANI in Fig. 4 show that it had low crystallinity.

Fig. 3 also shows that up to 53 wt%, the XRD patterns of the MCC/PANI nanocomposites were similar to those of the MCC. However, beyond 53 wt% PANI content, a shoulder appeared in the XRD patterns of the MCC/PANI nanocomposites at 2θ *ca.* 30°, which corresponds to a characteristic PANI peak. In the XRD patterns of the nanocomposites, the intensity of the characteristic MCC diffraction peak at *ca.* 27° was observed to decrease with an increase in the PANI content. This observation shows that the crystallinity of the nanocomposites decreased with an increase in the PANI content.

3.2 Cr(VI) adsorption by the MCC

The performance of the MCC as an adsorbent for the removal of the Cr(VI) from the synthetic wastewater was reported in

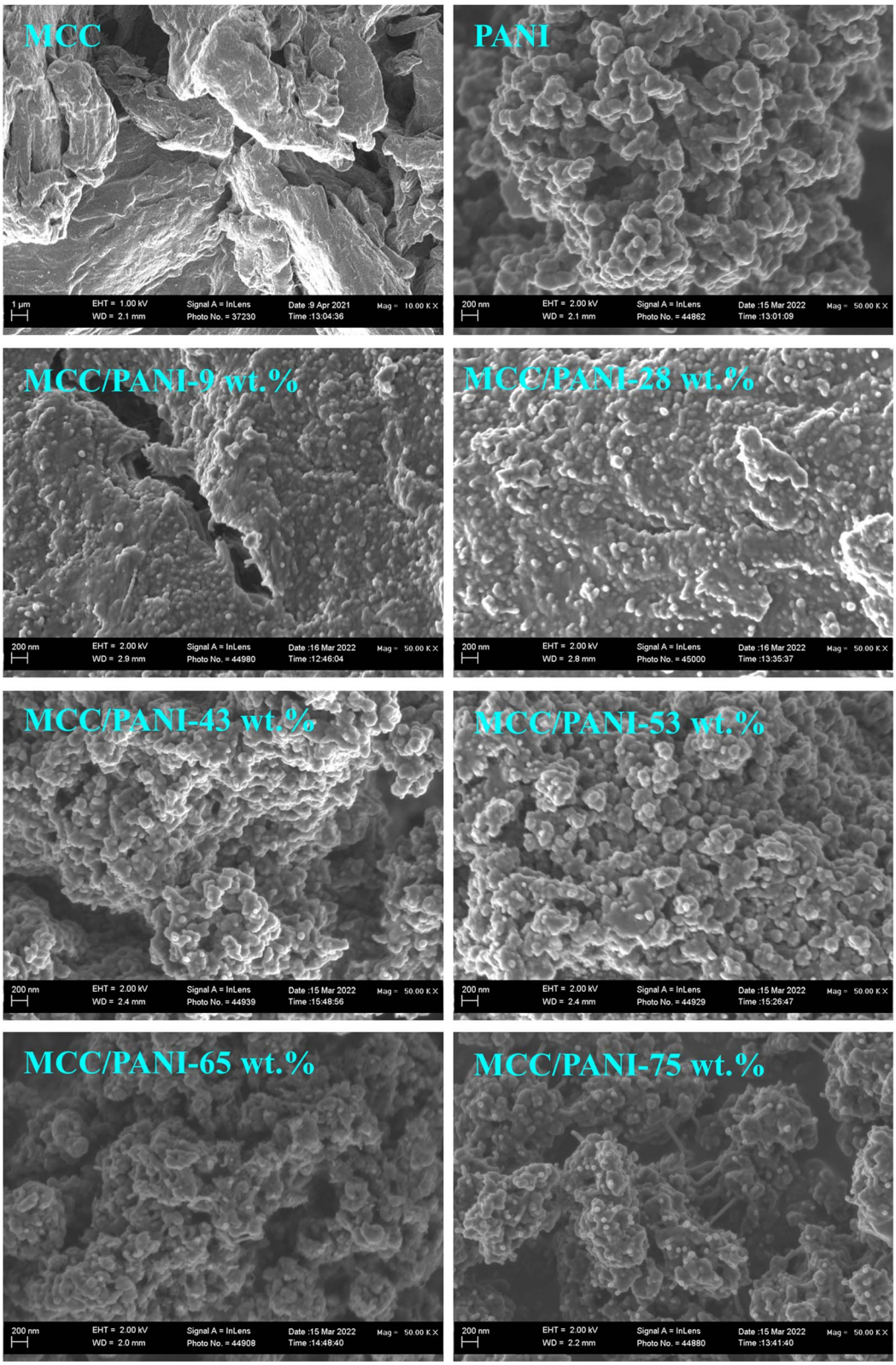

Fig. 2 SEM micrographs of MCC, PANI and MCC/PANI nanocomposites.

detail elsewhere.[19] In brief, the optimal parameters for the removal of the Cr(VI) from the synthetic wastewater by the MCC were determined to be an initial Cr(VI) concentration of 10 mg L^{-1}, an adsorbent dosage of 20 g L^{-1} and a Cr(VI) solution pH of 1. The MCC took 96 h to reach equilibrium and the equilibrium removal efficiency was 83%. The MCC

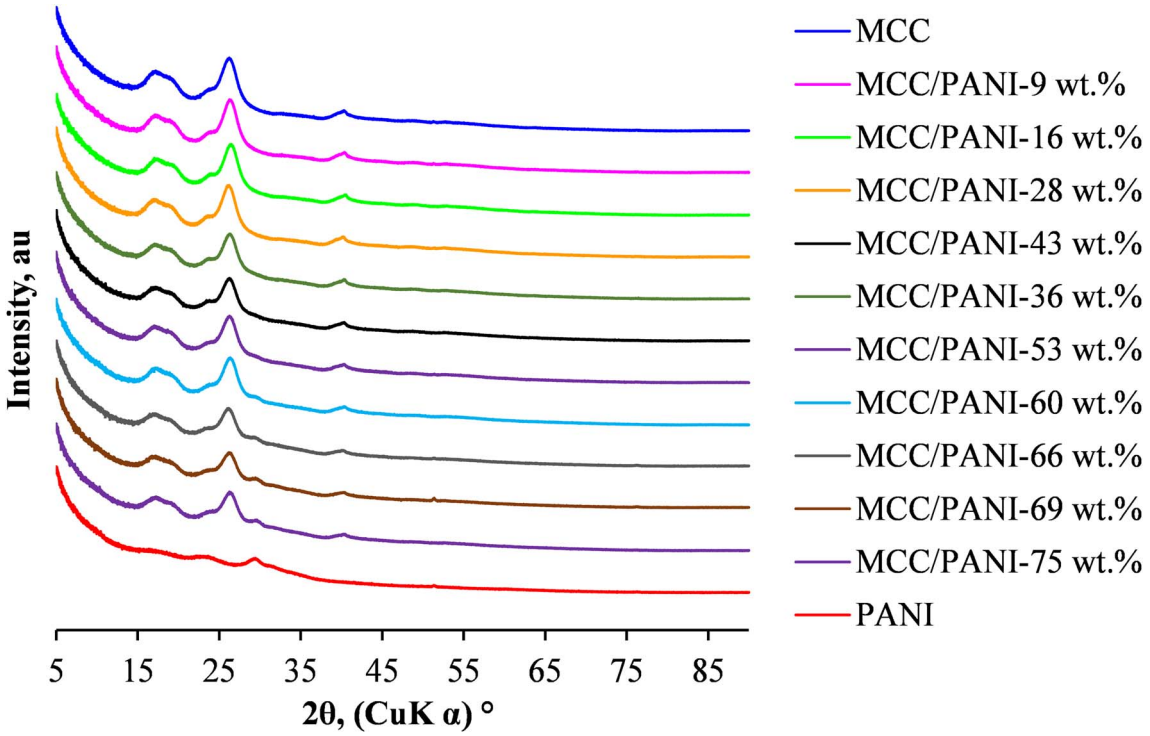

Fig. 3 X-ray diffraction patterns of MCC, PANI and MCC/PANI nanocomposites.

exhibited a point of zero charge of pH 6.2. The presence of Cr(III) in solution during the adsorption process suggested that the Cr(VI) removal mechanism from wastewater by the MCC was an adsorption coupled reduction mechanism. The kinetics data were best described by the pseudo second order (PSO) model and the Freundlich isotherm best fit the experimental equilibrium data. The adsorption capacity of the MCC was relatively lower at 3.92 mg g^{-1}, when compared to that of commercial adsorbents.[19,20]

3.3 Cr(VI) adsorption by the MCC/PANI nanocomposites

3.3.1 Effect of the PANI content and the adsorbent dosage on the Cr(VI) removal efficiency. Fig. 4(a) shows the variation of

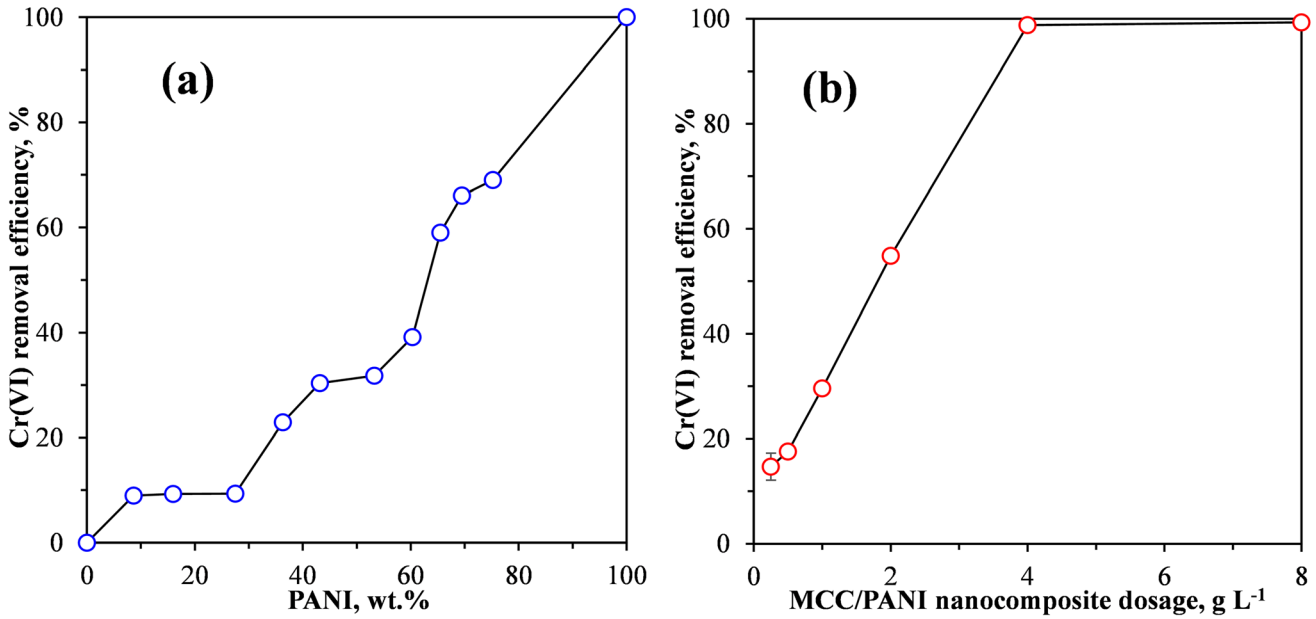

Fig. 4 Effect of (a) PANI content and (b) MCC/PANI nanocomposite adsorbent dosage on the Cr(VI) removal efficiency from synthetic wastewater by MCC/PANI nanocomposites.

the Cr(VI) removal efficiency from synthetic wastewater with PANI content in the MCC/PANI nanocomposites. In this experiment, the initial Cr(VI) concentration in the synthetic wastewater was 100 mg L^{-1}, the solution pH was 7 and the adsorbent dosage was 2 g L^{-1}.

Fig. 4(a) shows that under the conditions used, the Cr(VI) removal efficiency was less than 10% as the PANI content was increased from 0 to 28 wt%. It is also observed in Fig. 4(a) that under the same conditions, when the PANI content was increased from 28 wt% the Cr(VI) removal efficiency of the MCC/PANI nanocomposites increased with an increase in the PANI content, reaching a Cr(VI) removal efficiency of 30% at 43 wt% PANI content. A further increase in the PANI content to 53 wt% resulted in a marginal increase in the Cr(VI) removal efficiency of about 1%. However, the Cr(VI) removal efficiency increased once more with further increases in the PANI content, reaching 66% and 69% at PANI contents of 69 wt% and 75 wt% respectively. The MCC/PANI nanocomposite with 69 wt% was thus selected for further study.

The results presented in Fig. 4(a) appear to be consistent with the SEM and BET surface area results observed for the nanocomposites. The SEM results of the MCC/PANI nanocomposites presented in Fig. 2 show that for PANI contents up to 28 wt%, the PANI nanospheres uniformly covered the MCC surfaces. This resulted in the increase in the specific surface areas of the nanocomposites (Table 2). However, up to 28 wt% PANI, this increase in surface areas did not translate to high Cr(VI) removal efficiencies. Higher PANI contents beyond 28 wt% PANI resulted in the agglomeration of the PANI nanospheres on the MCC surfaces (Fig. 2). The agglomeration of the PANI particles on the MCC surface resulted in significantly higher specific surface areas, which apparently resulted in higher Cr(VI) removal efficiencies. Table 2 also shows that there was an 84% increase in the total pore volume of the MCC/PANI nanocomposites when the PANI content was increased from 28 wt% to 53 wt%. The increased pore volumes at higher PANI contents could also have contributed to high Cr(VI) removal efficiencies.

The effect of the adsorbent dosage on the removal efficiency of Cr(VI) by the MCC/PANI-69 wt% nanocomposite is shown in Fig. 4(b). This experiment was conducted using an initial Cr(VI) concentration of 100 mg L^{-1}, and a Cr(VI) solution pH of 7. Fig. 4(b) shows that there was a near linear increase in the Cr(VI) removal efficiency as the adsorbent dosage was increased from 0.25 to 4 g L^{-1}. The increase in the Cr(VI) removal efficiency with an increase in the adsorbent dosage was due to the increased number of available adsorption sites.

Fig. 4(b) shows that a 100% removal efficiency was observed at an adsorbent dosage of 4 g L^{-1}. Further increases in the adsorbent dosage did not result in any change, therefore 4 g L^{-1} was selected as the optimum adsorbent dosage for the MCC/PANI-69 wt% nanocomposite adsorbent, which was then used for further studies. In comparison, at a Cr(VI) solution of pH 7, the optimum adsorbent dosage for the removal of Cr(VI) by MCC was 20 g L^{-1}. The optimum MCC dosage of 20 g L^{-1} exhibited a Cr(VI) removal efficiency of only 23% after 120 h contact time, whereas the MCC/PANI-69 wt% optimum dosage of 4 g L^{-1} showed a Cr(VI) removal efficiency of 100% after 24 h, at a solution pH of 7. These observations show that modification of MCC with polyaniline decreased the adsorbent dosage required to effectively adsorb Cr(VI) and also enhanced its Cr(VI) removal efficiency.

3.3.2 Effect of initial Cr(VI) concentration on the Cr(VI) removal efficiency from synthetic wastewater by MCC/PANI nanocomposites. The effect of the initial Cr(VI) concentration on the Cr(VI) removal efficiency and adsorption capacity of the MCC/PANI nanocomposites was studied by varying the initial concentration of the synthetic wastewater from 100–500 mg L^{-1} using the MCC/PANI-69 wt% nanocomposite. For this experiment, the Cr(VI) solution pH was 7 and the optimum adsorbent loading of 4 g L^{-1} was used. The Cr(VI) solution was contacted with the adsorbent for 180 min at room temperature.

Fig. 5 shows that when the initial Cr(VI) concentration was 100 mg L^{-1}, the Cr(VI) removal efficiency of the Cr(VI) from the synthetic wastewater by the MCC/PANI-69 wt% nanocomposite was close to 100%, whereas the adsorption capacity was about 25 mg g^{-1}. In comparison, when the optimal MCC adsorbent dosage and pH of 20 g L^{-1} and 1, respectively were used with an initial Cr(VI) concentration of 100 mg L^{-1}, a Cr(VI) removal efficiency and adsorption capacity of about 60% and 3 mg g^{-1} were obtained respectively. The higher adsorption capacity exhibited by the MCC/PANI-69 wt%, compared to the MCC was possibly due to the increased specific surface area of the MCC/PANI nanocomposites, after modification and functionalization with PANI, which increased the number of available sites for the uptake of the Cr(VI) species.

Fig. 5 shows that when the synthetic wastewater had an initial Cr(VI) concentration of 100 mg L^{-1}, a Cr(VI) removal efficiency of 96.996% was achieved using the MCC/PANI-69 wt% nanocomposite adsorbent at a dosage of 4 g L^{-1} and a pH solution of 7. At this removal efficiency, the final Cr(VI) concentration of the

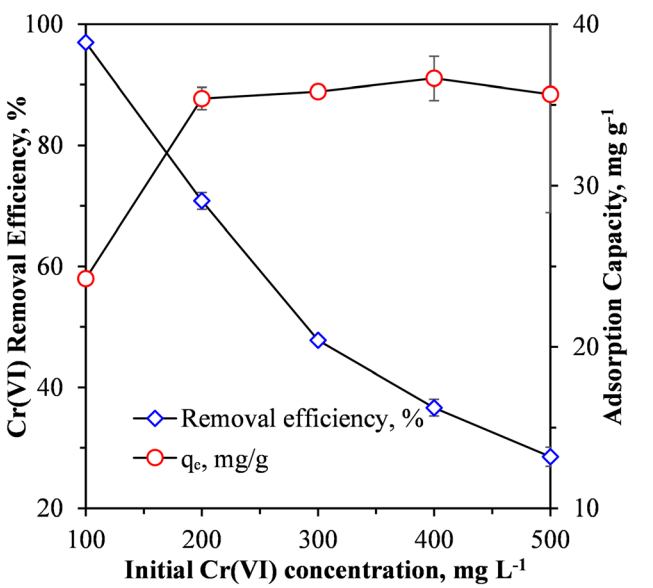

Fig. 5 Effect of initial Cr(VI) concentration on Cr(VI) removal efficiency and adsorption capacity of MCC/PANI-69 wt% nanocomposite.

treated water (3 mg L^{-1}) was higher than the recommended WHO recommended limit of 0.05 mg L^{-1}. However, Fig. 5 suggests that if the wastewater had an initial Cr(VI) concentration lower than 100 mg L^{-1}, the removal efficiency would be higher and the final Cr(VI) concentration of the treated water could approach the WHO recommended limit. However, further work will need to be conducted to confirm this premise.

The exponential decrease in the Cr(VI) removal efficiency with an increase in the initial Cr(VI) concentration observed in Fig. 5 is attributed to the saturation of adsorption sites on the MCC/PANI nanocomposite.

Fig. 5 also shows that the adsorption capacity of the nanocomposite increased from 25 mg g^{-1} to 36 mg g^{-1} with an increase in the initial Cr(VI) concentration from 100 mg L^{-1} to 200 mg L^{-1}. However, the adsorption capacity plateaued thereafter with an increase in the initial Cr(VI). The increase in the adsorption capacity was possibly due to the effective utilization of available active adsorption sites on the MCC/PANI nanocomposite surface, which was not possible at low initial Cr(VI) concentrations. The increase in adsorption capacity with an increase in the initial Cr(VI) could also have been due to higher mass transfer driving forces at higher initial Cr(VI) concentrations[34,35]

3.3.3 Effect of contact time and initial Cr(VI) concentration on the removal of Cr(VI) from synthetic wastewater by MCC/PANI nanocomposites. The results presented in Fig. 6 show the effect of contact time for the initial Cr(VI) concentrations 100, 200, and 300 mg L^{-1} on the removal of Cr(VI) from synthetic wastewater by the MCC/PANI-69 wt% nanocomposites. In these experiments, the Cr(VI) solution pH was 7, and the adsorbent dosage used was 4 g L^{-1}. These experiments were used to determine the equilibrium time and removal efficiency for the nanocomposite.

When pristine MCC was used as an adsorbent for the removal of Cr(VI) from the synthetic wastewater, the adsorption process was relatively slow, equilibrium was reached after 96 h at a Cr(VI) removal efficiency of 83%.[19] Fig. 6 shows that for the MCC/PANI-69 wt% nanocomposite, and for the three Cr(VI) initial concentrations considered (100, 200 and 300 mg L^{-1}), the Cr(VI) removal efficiencies increased rapidly in the first 10 min and then continued to increase slowly until equilibrium was reached at 30 min. The rapid Cr(VI) adsorption within the first 10 min demonstrated a high affinity of the Cr(VI) by the MCC/PANI adsorbent. The reduced increase observed in the Cr(VI) removal efficiencies in Fig. 6 after 10 min was probably due to the easily accessible active sites which were occupied first by Cr(VI) species becoming inaccessible and the remaining Cr(VI) species in solution finding it difficult to access adsorption sites.

Fig. 6 also shows that for the MCC/PANI-69 wt% nanocomposite, beyond the equilibrium times of 30 min, the Cr(VI) removal efficiency plateaued for all the initial Cr(VI) concentrations considered. This observation is attributed to the non-availability of adsorption sites on the adsorbent surface after most of them had already been occupied by the Cr(VI) species at the initial stage. A decreased concentration gradient of Cr(VI) could also have reduced mass transfer of Cr(VI) to the adsorbent surface.

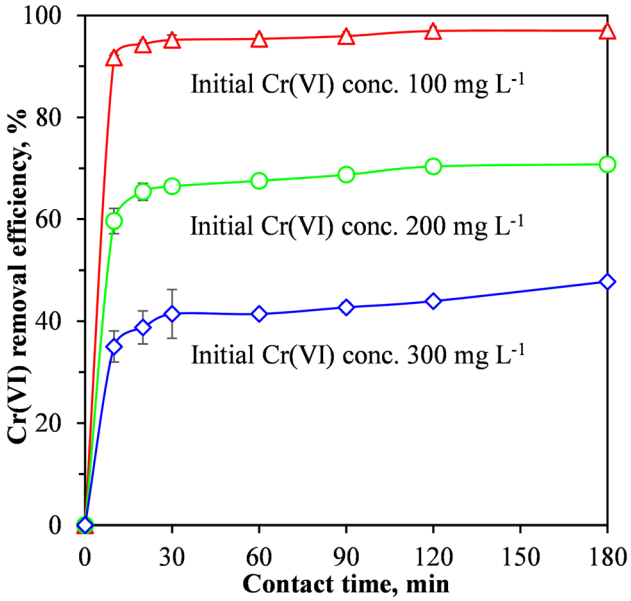

Fig. 6 Effect of contact time and initial concentration Cr(VI) concentration on the removal of Cr(VI) from wastewater using the MCC/PANI-69 wt% nanocomposite.

It was also observed in Fig. 6 that for the initial Cr(VI) concentrations of 100, 200 and 300 mg L^{-1}, the maximum Cr(VI) removal effectiveness were 95, 67 and 45% respectively, at the equilibrium time of 30 min.

3.3.4 Cr(VI) removal mechanism from wastewater by MCC/PANI nanocomposites. The FTIR spectroscopy results presented and discussed in section 3.1.1 suggest that the MCC interacted with PANI though hydrogen bonding, in agreement with observations from prior studies.[31] Hydrogen bonding between MCC and PANI was possibly through the OH groups of the MCC and unprotonated amine and imine groups of PANI. The FTIR spectroscopy results also suggest that the PANI synthesized in this study was present in the doped emaraldine salt form in which some of the amine and imine groups are protonated, both in its pristine form and also in the MCC/PANI nanocomposites.

Energy dispersive X-ray (EDX) analysis results presented in Table 3 show that both the neat PANI and the MCC/PANI-69 wt% contained significant amounts of nitrogen and sulphur. This is further evidence that PANI was successfully synthesized and that it was doped with PTSA. The sulphur was derived from the PTSA.[36]

The adsorption experiments conducted using the MCC/PANI-69 wt% were conducted at pH 7. The Cr(VI) speciation diagram shows that, at the initial Cr(VI) concentration of 100 mg L^{-1} used in the adsorption experiments, and at pH 7, the Cr(VI) was in the form of chromate anions, CrO_4^{2-}.[7] It is therefore inferred that removal of Cr(VI) from the synthetic wastewater occurred through electrostatic attraction between the CrO_4^{2-} anions and the protonated amines/imines of the PANI.

Jahan *et al.* previously studied the removal of Cr(VI) from solution at pH 7 using a PANI/bacterial cellulose (BC) mat.[37] They proposed that the removal mechanism consisted of three steps *viz.* adsorption of Cr(VI) onto the adsorbent surface,

Table 3 Elemental composition of MCC, PANI and MCC/PANI nanocomposites determined by EXD analysis

Element (at%)	MCC	PANI	MCC/PANI-69 wt%	MCC/PANI-69 wt% (after Cr(VI) adsorption)
O	100.00	73.08	73.42	66.37
N	—	15.37	12.63	8.50
S	—	11.55	13.95	4.95
Cr	—	—	—	20.17

reduction of the adsorbed Cr(VI) into Cr(III) on the PANI/BC mat, followed by desorption of Cr(III) into solution. The first step in the mechanism proposed by Jahan *et al.* is similar to the postulation from this study, that the negatively charged CrO_4^{2-} anions are removed by electrostatic attraction by the protonated amine and imine groups present in PANI.[37]

To determine whether reduction of Cr(VI) to Cr(III) occurred during the Cr(VI) removal process, the FTIR spectra of the nanocomposite adsorbent was studied before and after the adsorption process. Fig. 7 shows the FTIR spectra of the neat MCC, the as synthesized PANI and the MCC/PANI-69 wt% nanocomposite, and the MCC/PANI-69 wt% nanocomposite after contacting it with 100 mg L^{-1} Cr(VI) solution.

Fig. 7 shows that the relative intensities of the bands at *ca.* 1560 and 1460 cm^{-1} that are ascribed to the ring stretching of the quinoid (N=Q=N) and benzenoid (N–B–N) structures in PANI are higher in the MCC/PANI-69 wt% after it was exposed to the 100 ppm Cr(VI) solution, compared to the intensities of the same bands in the as synthesized PANI and the MCC/PANI-69 wt% nanocomposite. This is evidence that the PANI in the MCC/PANI-69 wt% nanocomposite which was in the emaraldine salt form was oxidised by the Cr(VI) into the pernigraniline form during the Cr(VI) removal process from the synthetic waste water. Simultaneously, the Cr(VI) was reduced into Cr(III).[38]

EDX analysis of the MCC/PANI-69 wt% adsorbent after exposure to the Cr(VI) solution confirmed the presence of Cr on its surface (Table 3). This Cr must have been Cr(III) that precipitated on the nanocomposite adsorbent. In summary, it is postulated that the Cr(VI) removal mechanism by the MCC/PANI-69 wt% nanocomposites at pH 7 was through electrostatic attraction of Cr(VI) species by protonated amine and amine groups of PANI, reduction of Cr(VI) into Cr(III) and precipitation of Cr(III) on the nanocomposite surface.

3.3.5 Adsorption kinetics of the Cr(VI) removal by MCC/PANI nanocomposites. To investigate the adsorption kinetics of the Cr(VI) removal by MCC/PANI nanocomposites, the pseudo-second-order (PSO) kinetics model was fitted to the adsorption kinetics data for the removal of Cr(VI) by the MCC/

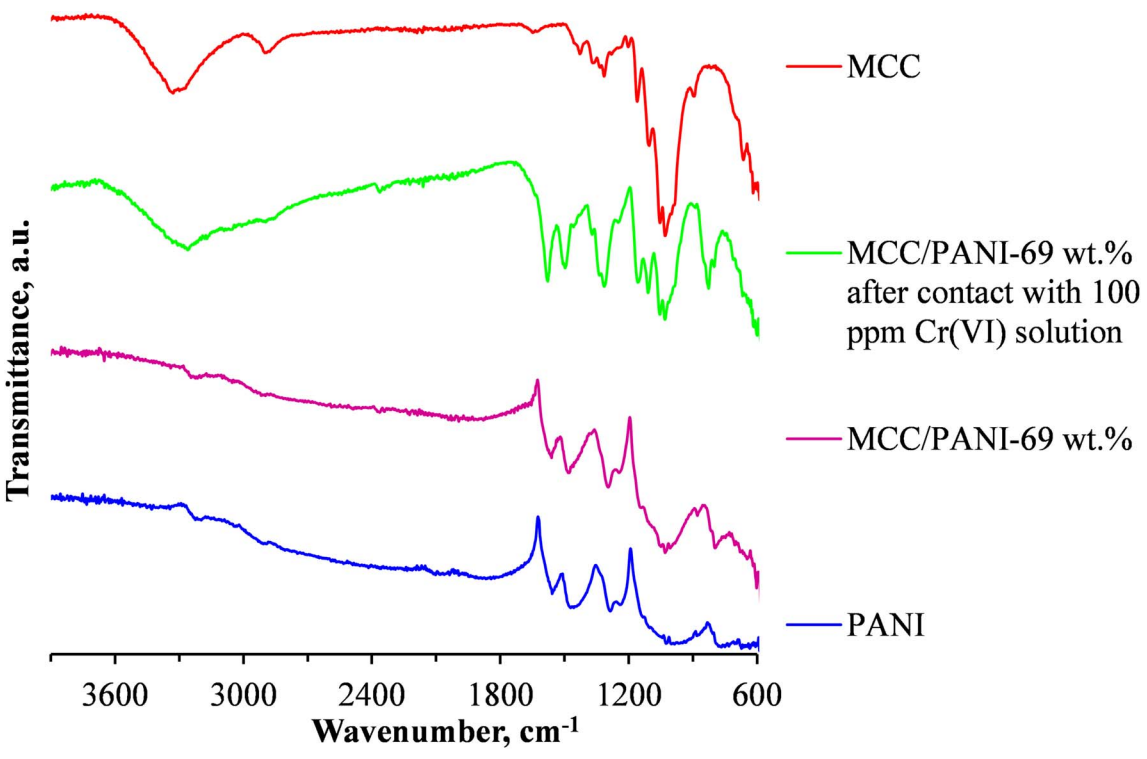

Fig. 7 FTIR spectra of MCC, PANI, MCC/PANI-69 wt% nanocomposites as synthesized and MCC/PANI-69 wt% nanocomposites after contact with 100 mg L^{-1} Cr(VI) solution.

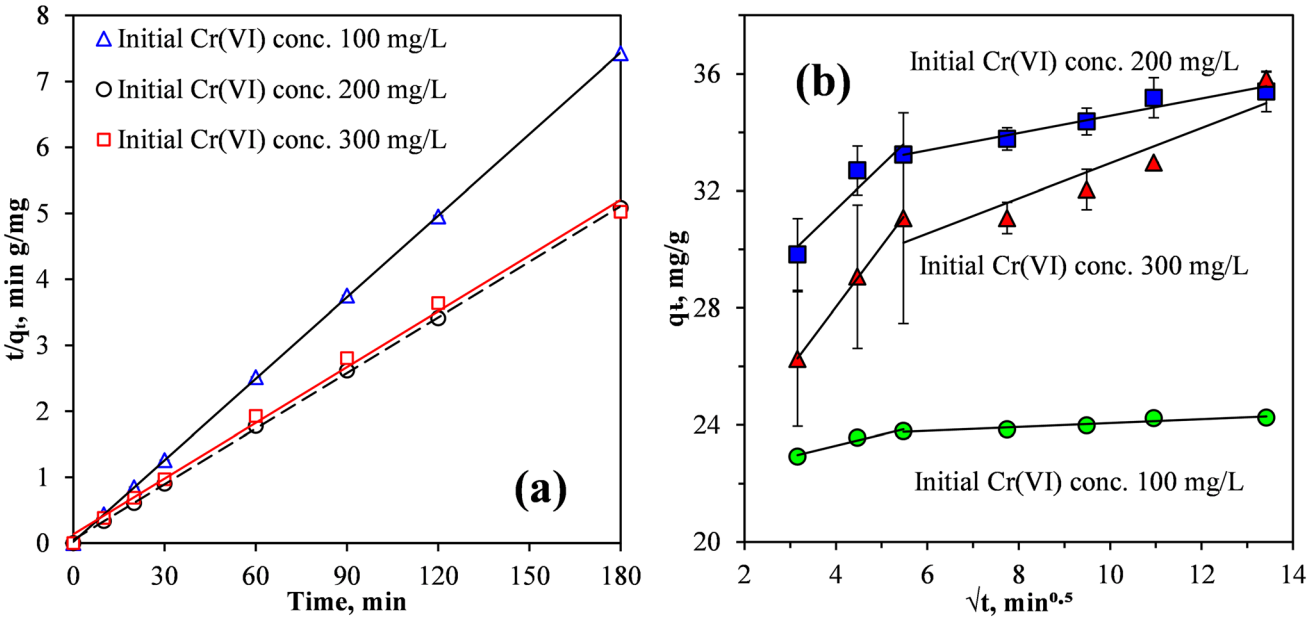

Fig. 8 Fits of (a) the PSO model and (b) the Webber–Morris intraparticle diffusion model to the kinetics data of Cr(VI) removal from synthetic wastewater by MCC/PANI-69 wt% nanocomposites at varying Cr(VI) initial concentrations.

PANI-69 wt% nanocomposite. The linear form of the PSO model as given in eqn (3) was used:[39]

$$\frac{t}{q_t} = \frac{1}{k_2 q_e^2} + \frac{t}{q_e} \quad (3)$$

In eqn (3), q_t and q_e are the adsorption capacities at time t (min), and at equilibrium (mg g^{-1}), respectively. k_2 is the pseudo second order rate constant (g mg^{-1} min^{-1}).

The Weber–Morris intra-particle diffusion model given in eqn (4) was also employed to investigate the rate controlling mechanism of Cr(VI) adsorption onto the MCC/PANI-69 wt% nanocomposite. The Weber and Morris Model is given as follows:[40]

$$q_t = k_{id} t^{1/2} + C \quad (4)$$

where q_t is the adsorption capacity (mg g^{-1}) at contact time t (min), k_{id} is the intraparticle diffusion rate coefficient (g mg^{-1} $min^{-1/2}$) and C is a constant that reflects the boundary layer effect or surface adsorption.[40,41]

In the Cr(VI) adsorption kinetics studies, initial Cr(VI) solution concentrations of 100, 200 and 300 mg L^{-1} at pH 7.0 were used, and the optimum adsorbent dosage of 4 g L^{-1} was used. The appropriateness of the kinetics models in describing the experimental data were determined by evaluating the linear regression correlation coefficient (R^2) of the fits.

Fig. 8(a) shows the fits of the PSO model to the kinetics data of Cr(VI) removal by the MCC/PANI-69 wt% nanocomposites from the synthetic wastewater. The parameters determined in fitting the models are given in Table 4.

Fig. 8(a) and the correlation coefficients, R^2, presented in Table 4 confirmed that the kinetics data correlated well with the PSO model, for the three initial Cr(VI) concentrations considered. Also, the equilibrium adsorption capacities q_e, determined using the PSO model, were very close to the experimental values for the three initial Cr(VI) concentrations considered. Thus, the PSO model provided an appropriate fit to the experimental kinetics data for the removal of the Cr(VI) from the synthetic wastewater by the MCC/PANI-69 wt% nanocomposites. This agrees with several previous studies in which the PSO model provided good fits to describe adsorption kinetics for metals such as Cr(VI) from aqueous solutions.[42–44] A good fit of the experimental data to the PSO model is evidence that the adsorption mechanism was due to the chemisorption.[41,44]

Fig. 8(b) show fits of the Weber and Morris intraparticle diffusion model to the Cr(VI) removal data by the MCC/PANI-69 wt% nanocomposite at varying Cr(VI) initial concentrations. The Weber and Morris model is frequently used to identify the adsorption mechanism(s) and to predict the rate-controlling step in adsorption processes. It is apparent from Fig. 8(b) that plots of q_t against $t^{1/2}$ for the three initial concentrations considered are not straight lines that pass through the origin. However, linear segments can be identified in the plots, for the three initial Cr(VI) concentrations. It can thus be concluded from Fig. 8(b) that Cr(VI) removal from solution by the MCC/PANI-69 wt% nanocomposite was controlled by multiple processes.[40,44,45] This agrees with the postulation made in § 3.3.4.

3.3.6 Adsorption isotherms for the Cr(VI) from synthetic water removal by MCC/PANI nanocomposites. The Langmuir isotherm in its linearized form as given in eqn (5) was fitted to the adsorption equilibrium data in an attempt to describe the Cr(VI) adsorption characteristics of the MCC/PANI-69 wt% nanocomposite.[46]

$$\frac{C_e}{q_e} = \frac{C_e}{q_m} + \frac{1}{K_L q_m} \quad (5)$$

Table 4 Parameters determined in fitting the PSO model to the kinetics data for the removal of Cr(VI) from synthetic wastewater by MCC/PANI-69 wt% nanocomposite

		Constants		
		Initial Cr(VI) concentrations		
Kinetics model	Parameter	100 mg L^{-1}	200 mg L^{-1}	300 mg L^{-1}
Pseudo second order	q_e, cal (mg g^{-1})	24.2718	35.8423	34.1297
	k (g mg^{-1} min^{-1})	0.06985	0.01383	0.00911
	h (mg g^{-1} min^{-1})	41.1525	17.7614	10.6157
	R^2	1	0.9996	0.9955
Experimental value	$q_{e,\ exp}$ (mg g^{-1})	24.2489	35.671	35.8333

In eqn (5), C_e is the equilibrium concentration of Cr(VI) (mg L^{-1}), K_L is the Langmuir equilibrium adsorption constant (L mg^{-1}), q_e is the equilibrium adsorption capacity (mg g^{-1}), q_m is the maximum adsorption capacity (mg g^{-1}).

Fig. 9 shows a fit of the Langmuir adsorption isotherm to the equilibrium adsorption data for the removal of Cr(VI) by the MCC/PANI-69 wt% nanocomposite. The parameters determined from fitting the Langmuir isotherm are presented in Table 5.

Fig. 9 and Table 5 show that the Langmuir isotherm provided a good fit to the experimental data for the Cr(VI) removal from the synthetic wastewater by the MCC/PANI-69 wt% nanocomposite. The Langmuir isotherm had a relatively higher correlation coefficient (0.9996) showing that it adequately described the experimental data for the Cr(VI) removal from the wastewater by the MCC/PANI-69 wt% nanocomposite. This observation suggests that the removal of the Cr(VI) by the MCC/PANI-69 wt% nanocomposite occurred through monolayer adsorption.[46,47] The maximum monolayer adsorption capacity of the MCC/PANI-69 wt% nanocomposite adsorbent was 36.10 mg g^{-1} (Table 5).

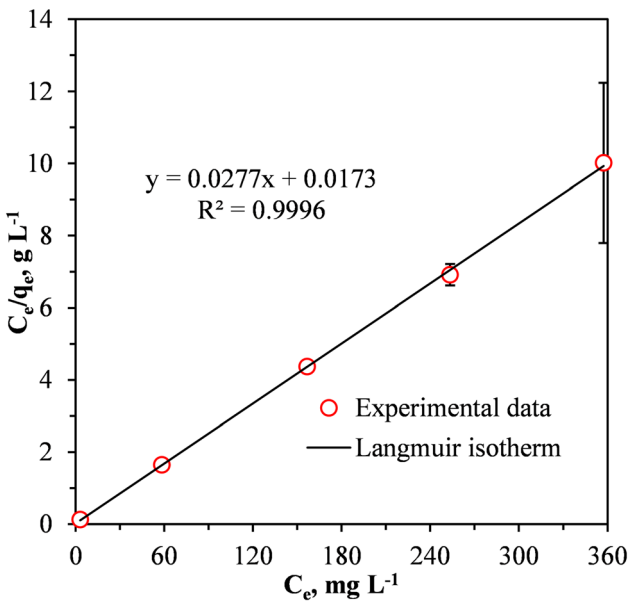

Fig. 9 Linear fit of the Langmuir isotherm model to the data for the adsorption of Cr(VI) by the MCC/PANI-69 wt% nanocomposite.

Table 5 Langmuir isotherm parameters for the adsorption of Cr(VI) by the MCC/PANI-69 wt% nanocomposite

Isotherm	Parameter	Value
Langmuir	q_m (mg g^{-1})	36.1011
	K_L (L mg^{-1})	1.6012
	R^2	0.9996

The separation factor R_L values which are related to the Langmuir isotherm, where between 0 and 1 for the three initial Cr(VI) concentrations, this confirms that adsorption of the Cr(VI) by MCC/PANI-69 wt% nanocomposite was favourable.[48]

3.3.7 Comparison of the maximum adsorption capacity of the MCC/PANI-69 wt% nanocomposite with other adsorbents considered for the removal of Cr(VI) from water. The maximum adsorption capacity of the MCC used in this study for Cr(VI) removal from synthetic wastewater was previously determined as 3.917 mg g^{-1}, at pH 1. This value was significantly low compared to those of commercial adsorbents.[20] In this study the MCC was modified through *in situ* polymerization of aniline to yield MCC/PANI nanocomposite adsorbents. The MCC/PANI-69 wt% nanocomposite exhibited a significantly improved monolayer maximum adsorption capacity of 35.97 mg g^{-1}, at pH 7 (Table 5). The adsorption capacity of 35.97 mg g^{-1} for Cr(VI) exhibited by the MCC/PANI-69 wt% nanocomposite in this study was comparable to other modified and functionalized adsorbents based on cellulose.[49,50] However, this adsorption capacity was significantly lower compared to that of the amine modified adsorbent based on MCC.[51] This adsorption capacity was also relatively high when compared to several forms of activated carbons and other low-cost adsorbents for Cr(VI) removal, signifying good performance.[7] It is however important to note that the adsorption capacity of 35.97 mg g^{-1} exhibited by the MCC/PANI-69 wt% nanocomposite in this study was obtained at pH 7, unlike most of the other adsorbents, which require low pH values to attain their maximum adsorption capacities.[7]

4 Conclusions

FTIR and XRD analysis confirmed the successful *in situ* chemical oxidative polymerization of aniline on the MCC surfaces.

SEM showed that MCC was an effective scaffold for PANI synthesis. The agglomeration of the PANI nanospheres on the MCC surfaces apparently enhanced the specific surface area of the MCC/PANI nanocomposites compared to the neat MCC. Batch adsorption studies showed that the optimal conditions for the removal of Cr(VI) from synthetic wastewater using the MCC/PANI-69 wt% nanocomposite as an adsorbent were an initial Cr(VI) concentration of 100 mg L^{-1}, an adsorbent dosage of 4 g L^{-1} and a Cr(VI) solution pH of 7. The MCC/PANI-69 wt% required only 30 min to reach equilibrium and it attained an equilibrium removal efficiency of 95%.

FTIR analysis suggested that the Cr(VI) removal mechanism by the MCC/PANI-69 wt% nanocomposites at pH 7 was through electrostatic attraction of the CrO_4^{2-} anions by protonated amine and amine groups of PANI, reduction of the adsorbed Cr(VI) into Cr(III) and precipitation of Cr(III) on the nanocomposite surface. EDX analysis of the MCC/PANI-69 wt% adsorbent after exposure to the Cr(VI) solution confirmed the presence of Cr on its surface, also supporting the proposed mechanism.

Good fits of the PSO model to the experimental kinetics data for the removal of the Cr(VI) from the synthetic wastewater by the MCC/PANI-69 wt% nanocomposite implied that the adsorption process involved chemisorption. Fits of the Weber and Morris intraparticle diffusion model to the kinetics data for Cr(VI) removal by the MCC/PANI-69 wt% nanocomposite at varying Cr(VI) initial concentrations confirmed that Cr(VI) removal from solution by the MCC/PANI-69 wt% nanocomposite was controlled by multiple processes, in agreement with the postulated removal mechanism. The Langmuir isotherm best described the experimental data for the Cr(VI) removal from the wastewater by the MCC/PANI-69 wt% nanocomposite, suggesting that the removal of the Cr(VI) by the MCC/PANI-69 wt% nanocomposite occurred through monolayer adsorption.

The MCC/PANI-69 wt% nanocomposite exhibited a significantly improved monolayer maximum adsorption capacity of 36.10 mg g^{-1}, at pH 7, in comparison to that of the MCC (3.92 mg g^{-1} at pH 1). The MCC/PANI-69 wt% nanocomposite maximum adsorption capacity was comparable to other modified and functionalized adsorbents based on cellulose. The relatively high adsorption capacity of the MCC/PANI-69 wt% nanocomposite was attributed to its significantly higher specific surface area after modification of the MCC with the PANI. The amine and imine functional groups of the PANI also effectively interacted with the Cr(VI), enhancing its adsorption capacity. An important result from the study was that whereas most of the reported adsorbents for Cr(VI) are only effective at low pH values, the MCC/PANI nanocomposite synthesized in this study was effective at pH 7.

Data availability

The datasets generated during and/or analysed during the current study are available from the corresponding author on reasonable request.

Author contributions

Conceptualization: [Washington Mhike]; methodology: [Washington Mhike], [Shepherd M. Tichapondwa]; formal analysis and investigation: [Lovejoy Dewa]; writing – original draft preparation: [Lovejoy Dewa]; writing – review and editing [Washington Mhike], [Shepherd Tichapondwa]; funding acquisition [Washington Mhike]; resources [Washington Mhike], [Shepherd M. Tichapondwa]; supervision: [Washington Mhike], [Shepherd M. Tichapondwa].

Conflicts of interest

The authors have no competing interests to declare that are relevant to the content of this article.

Acknowledgements

Open access funding was provided by Tshwane University of Technology. Samantha Govender and Rettenmaier South Africa are acknowledged for providing the MCC used in this study, at no cost. Financial support by the Department of Science and Innovation, South Africa, through the Paper Manufacturers Association of South Africa under Grant DST/CON 004/2019 is acknowledged.

References

1 R. Saha, R. Nandi and B. Saha, *J. Coord. Chem.*, 2011, **64**, 1782–1806.
2 M. Loock-Hattingh, PhD in Chemistry, North-West University, 2016.
3 H.-J. Lunk, *ChemTexts*, 2015, **1**, 1–17.
4 P. B. Tchounwou, C. G. Yedjou, A. K. Patlolla and D. J. Sutton, in *Molecular, Clinical and Environmental Toxicology. Experientia Supplementum*, ed. A. Luch, Springer, Basel, 2012, vol. 101, pp. 133–164.
5 Z. Rahman and V. P. Singh, *Environ. Monit. Assess.*, 2019, **191**, 419.
6 P. Sharma, S. P. Singh, S. K. Parakh and Y. W. Tong, *Bioengineered*, 2022, **13**, 4923–4938.
7 D. Mohan and C. U. Pittman, *J. Hazard. Mater.*, 2006, **137**, 762–811.
8 S. K. Sharma, B. Petrusevski and G. Amy, *J. Water Supply: Res. Technol.-AQUA*, 2008, **57**, 541–553.
9 P. J. Williams, E. Botes, M. M. Maleke, A. Ojo, M. F. DeFlaun, J. Howell, R. Borch, R. Jordan and E. van Heerden, *Water S.A.*, 2014, **40**, 549–554.
10 N. Kumar, A. Kardam, V. Jain and S. Nagpal, *Sep. Sci. Technol.*, 2020, **55**, 1436–1448.
11 F. Fu and Q. Wang, *J. Environ. Manage.*, 2011, **92**, 407–418.
12 M. E. González-López, C. M. Laureano-Anzaldo, A. A. Pérez-Fonseca, M. Arellano and J. R. Robledo-Ortíz, *Sep. Purif. Rev.*, 2021, **50**, 333–362.
13 V. K. Gupta, A. Nayak and S. Agarwal, *Environ. Eng. Res.*, 2015, **20**, 1–18.

14 G. Crini, E. Lichtfouse, L. D. Wilson and N. Morin-Crini, *Environ. Chem. Lett.*, 2019, **17**, 195–213.
15 I. Michalak, K. Chojnacka and A. Witek-Krowiak, *Appl. Biochem. Biotechnol.*, 2013, **170**, 1389–1416.
16 C. Olsson and G. Westman, in *Cellulose*, ed. T. van de Ven and L. Godbout, IntechOpen, Rijeka, 2013, ch. 6, p. 52144.
17 P. M. Ejikeme, *Cellulose*, 2008, **15**, 141–147.
18 A. Jamshaid, A. Hamid, N. Muhammad, A. Naseer, M. Ghauri, J. Iqbal, S. Rafiq and N. S. Shah, *ChemBioEng Rev.*, 2017, **4**, 240–256.
19 W. Mhike, L. Dewa and S. Tichapondwa, *Chem. Eng. Trans.*, 2023, **103**, 661–666.
20 Z. N. Garba, I. Lawan, W. Zhou, M. Zhang, L. Wang and Z. Yuan, *Sci. Total Environ.*, 2020, **717**, 135070.
21 S. Bhadra, D. Khastgir, N. K. Singha and J. H. Lee, *Prog. Polym. Sci.*, 2009, **34**, 783–810.
22 I. Y. Sapurina, M. A. Shishov and V. T. Ivanova, *Russ. Chem. Rev.*, 2020, **89**, 1115.
23 H. Hajjaoui, A. Soufi, W. Boumya, M. Abdennouri and N. Barka, *J. Compos. Sci.*, 2021, **5**, 233.
24 S. N. Benaouda, H. Chaker, F. Abidallah, C. Bachir, H. Tawheed, P. G. Weidler, A. Bengueddach, J. Canales-Vázquez and R. Hamacha, *J. Porous Mater.*, 2022, 1–15.
25 J. Stejskal, D. Hlavatá, P. Holler, M. Trchová, J. Prokeš and I. Sapurina, *Polym. Int.*, 2004, **53**, 294–300.
26 E. N. Bakatula, D. Richard, C. M. Neculita and G. J. Zagury, *Environ. Sci. Pollut. Res.*, 2018, **25**, 7823–7833.
27 *Standard Methods for the Examination of Water and Wastewater*, ed. A. D. Eaton and M. A. H. Franson, American Public Health Association, 2005.
28 A. John, S. K. Mahadeva and J. Kim, *Smart Mater. Struct.*, 2010, **19**, 045011.
29 V. P. Anju and S. K. Narayanankutty, *Polym. Bull.*, 2019, **76**, 5253–5267.
30 M. Babazadeh, *Iran. Polym. J.*, 2007, **16**, 389–396.
31 J. Li, X. Qian, L. Wang and X. J. B. An, *BioResources*, 2010, **5**, 712–726.
32 J. Stejskal, I. Sapurina, M. Trchová and E. N. Konyushenko, *Macromolecules*, 2008, **41**, 3530–3536.
33 N. Terinte, R. Ibbett and K. C. Schuster, *Lenzinger Ber.*, 2011, **89**, 118–131.
34 B. V. Babu and S. Gupta, *Adsorption*, 2008, **14**, 85–92.
35 M. T. Yagub, T. K. Sen, S. Afroze and H. M. Ang, *Adv. Colloid Interface Sci.*, 2014, **209**, 172–184.
36 M. V. Kulkarni, A. K. Viswanath, R. C. Aiyer and P. K. Khanna, *J. Polym. Sci., Part B: Polym. Phys.*, 2005, **43**, 2161–2169.
37 K. Jahan, N. Kumar and V. Verma, *Environ. Sci.: Water Res. Technol.*, 2018, **4**, 1589–1603.
38 X. L. Ma, G. T. Fei and S. H. Xu, *Nanoscale Res. Lett.*, 2021, **16**, 58.
39 Y.-S. Ho and G. McKay, *Process Biochem.*, 1999, **34**, 451–465.
40 J. Wang and X. Guo, *J. Hazard. Mater.*, 2020, **390**, 122156.
41 A. Pholosi, E. B. Naidoo and A. E. Ofomaja, *S. Afr. J. Chem. Eng.*, 2020, **32**, 39–55.
42 Y. Zheng, W. Wang, D. Huang and A. Wang, *Chem. Eng. J.*, 2012, **191**, 154–161.
43 M. O. Ansari, R. Kumar, S. A. Ansari, S. P. Ansari, M. Barakat, A. Alshahrie and M. H. Cho, *J. Colloid Interface Sci.*, 2017, **496**, 407–415.
44 T. H. Tran, H. Okabe, Y. Hidaka and K. Hara, *Carbohydr. Polym.*, 2017, **157**, 335–343.
45 H. Qiu, L. Lv, B.-c. Pan, Q.-j. Zhang, W.-m. Zhang and Q.-x. Zhang, *J. Zhejiang Univ., Sci., A*, 2009, **10**, 716–724.
46 X. Guo and J. Wang, *J. Mol. Liq.*, 2019, **296**, 111850.
47 D. D. Milenković, M. M. Milosavljević, A. D. Marinković, V. R. Đokić, J. Z. Mitrović and A. L. Bojić, *Water S.A.*, 2013, **39**, 515–522.
48 M. Gouamid, M. R. Ouahrani and M. B. Bensaci, *Energy Procedia*, 2013, **36**, 898–907.
49 B. Qiu, C. Xu, D. Sun, H. Yi, J. Guo, X. Zhang, H. Qu, M. Guerrero, X. Wang, N. Noel, Z. Luo, Z. Guo and S. Wei, *ACS Sustainable Chem. Eng.*, 2014, **2**, 2070–2080.
50 Y. Hao, Z. Cui, H. Yang, G. Guo, J. Liu, Z. Wang, A. Deniset-Besseau and S. Remita, *Cellul. Chem. Technol.*, 2018, **52**, 485–494.
51 F. Xue, H. He, H. Zhu, H. Huang, Q. Wu and S. Wang, *Langmuir*, 2019, **35**, 12636–12646.